

Combined effects of elevated temperatures and high strain rates on compressive performance of S30408 austenitic stainless steel

Li, Lijun; Wang, Rui; Zhao, Hui; Zhang, Haoran; Yan, Rui

DOI

[10.1016/j.istruc.2021.07.063](https://doi.org/10.1016/j.istruc.2021.07.063)

Publication date

2021

Document Version

Final published version

Published in

Structures

Citation (APA)

Li, L., Wang, R., Zhao, H., Zhang, H., & Yan, R. (2021). Combined effects of elevated temperatures and high strain rates on compressive performance of S30408 austenitic stainless steel. *Structures*, 34, 1-9. <https://doi.org/10.1016/j.istruc.2021.07.063>

Important note

To cite this publication, please use the final published version (if applicable). Please check the document version above.

Copyright

Other than for strictly personal use, it is not permitted to download, forward or distribute the text or part of it, without the consent of the author(s) and/or copyright holder(s), unless the work is under an open content license such as Creative Commons.

Takedown policy

Please contact us and provide details if you believe this document breaches copyrights. We will remove access to the work immediately and investigate your claim.



Combined effects of elevated temperatures and high strain rates on compressive performance of S30408 austenitic stainless steel

Lijun Li^a, Rui Wang^a, Hui Zhao^{a,b,*}, Haoran Zhang^a, Rui Yan^c

^a College of Civil Engineering, Taiyuan University of Technology, Taiyuan, China

^b Department of Civil Engineering, Tianjin University, Tianjin, China

^c Faculty of Civil Engineering and Geosciences, Delft University of Technology, Netherlands

ARTICLE INFO

Keywords:

S30408 austenitic stainless steel
Elevated temperatures
Dynamic response
Strain rate
Constitutive model

ABSTRACT

This paper presents an experimental investigation on the dynamic mechanical performance of S30408 austenitic stainless steel (ASS) under elevated temperatures, which is essential for determining the behaviour of structures made with this type of steel subjected to the coupled fire and impact/explosion. For this purpose, the quasi-static and dynamic compression tests using Split Hopkinson Pressure Bar (SHPB) were conducted under temperatures of 20–600 °C and strain rates from 0.001 to 3000 s⁻¹. In addition, the corresponding microstructures of tested samples were observed. The stress–strain responses, strain rate and temperature effects as well as the microstructural evolutions were analyzed. Test results show that the stress–strain responses are sensitive to the strain rate and temperature. The strain-rate sensitivity coefficient increases as the strain rate and temperature rise. The microstructural observation reveals that the grain dimension declines with an increment of strain rate or a decreasing temperature. Finally, the dynamic compressive stress–strain models for S30408 ASS under 20–600 °C were suggested on the basis of the Johnson-Cook (J-C) model and have been proved to give a reasonable prediction.

1. Introduction

In the last decades, 304 austenitic stainless steel (ASS) has been increasingly used in engineering structures [1–6]. It has several advantages compared to carbon steel, such as high corrosion resistance and durability, maintenance, improved fire and impact/blast resistance, etc. Due to these benefits, it is expected to be widely employed in the modern construction field, especially considering the life-cycle cost. Several design codes have been developed to regulate the use of the stainless steel in civil engineering, such as CECS 410:2015 [7] and EN 1993–1-4 [8]. Until now, the material and structural behaviours of 304 ASS subjected to the single static, dynamic, cyclic and fire conditions are relatively well understood [1–6,9–20]. In addition to the loading conditions mentioned above, the structures may suffer combined fire and impact/explosion action during the lifetime [21,22], such as 9.11 terrorist attack and Qingdao pipeline leak explosion. The fire may easily result in an explosion or progressive collapse, as presented in Fig. 1. Under such condition, the temperature effect on the behaviours of structural material should be considered when analyzing the dynamic responses of structures under impact loading. Therefore, it is essential to

systematically investigate the mechanical performance and microstructural characteristic of 304 ASS exposed to both high temperatures and strain rates in order to ensure the safety of 304 ASS structures subjected to such harsh environment.

For 304 ASS, the quasi-static mechanical performance at elevated temperatures and the dynamic mechanical properties at ambient temperature have been extensively examined [9,10,16,18]. Results demonstrate that temperature causes a significant decrease in material strength, whereas the high strain rate induces a strengthening effect on the yield stress at ambient temperature. EN 1993–1-2 [23] suggests that the nominal yield stress declines by about 50% when the temperature reaches 600 °C. Compared to carbon steel, stainless steel presents better high-temperature performance. As for the effect of strain rate at ambient temperature, a pronounced increase in the nominal yield stress exists provided that the strain rates exceed 10³ s⁻¹, owing to an enhanced rate of dislocation generation. Jia et al. [18] found that the dynamic yield strength of S30408 ASS under strain rate of 6212 s⁻¹ can reach up to approximate 3 times of that under quasi-static load.

Current results indicate that the mechanical properties of stainless steel are temperature and strain rate sensitive. Given the coupled

* Corresponding author at: College of Civil Engineering, Taiyuan University of Technology, Taiyuan, China.

E-mail address: zhaohui01@tyut.edu.cn (H. Zhao).

<https://doi.org/10.1016/j.istruc.2021.07.063>

Received 11 June 2021; Received in revised form 12 July 2021; Accepted 20 July 2021

Available online 28 July 2021

2352-0124/© 2021 Institution of Structural Engineers. Published by Elsevier Ltd. All rights reserved.

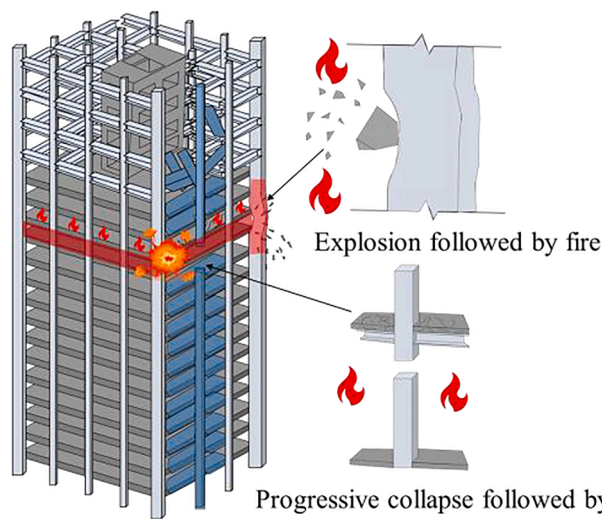


Fig. 1. Schematic view of explosion or progressive collapse followed by a fire.

temperature and dynamic loadings, the strengthening induced by the high strain rate and the thermal softening may complicate the stress–strain responses. Though previous researches on the 304 ASS have covered material and structural levels, the information on the coupled influences of high strain rates and elevated temperatures is still limited. Lee et al. [24,25] investigated the compressive performance and microstructure change of 304L ASS considering the influences of strain rate, temperature and pre-strain. Test strain rates and temperatures were set in the range of 2000–6000 s^{-1} and 300–800 $^{\circ}C$, respectively. It is concluded that the strain-rate sensitivity increases with rising strain rates and the descending temperatures. The microstructural observation indicated that the change in the flow stress under combined high strain rates and temperatures is related to the quantity of martensite and the densities of both dislocation and twin. Cadoni and Forni [26] studied the influences of strain rate and temperature on the mechanical responses of cold-formed AISI 304 ASS bars. Experiments were conducted using a split-Hopkinson tension bar under temperatures up to 1000 $^{\circ}C$ and 3 strain rates (250, 400 and 800 s^{-1}). They found that the yield stress decreases with the increasing temperatures and increases with an increment of the strain rate. Finally, the parameters of the Johnson-Cook (J-C) and Cowper-Symonds (C-S) models were determined. In 2020, Yang et al. [27] conducted SHPB tests to analyze the influences of strain rate and temperature on the compressive performance of ASTM A240/A240M 304 stainless steel. Due to the increased carbon content, the quasi-static yield stress achieves 702 MPa at room temperature. Additionally, the modified J-C model was suggested according to the test results. Table 1 summarizes the detailed information in literatures [24–27]. As mentioned previously, the existing researches are not sufficient to fully understand the performance of 304 ASS under combined high temperatures and high strain-rate conditions because of the different chemical compositions and test conditions.

In this context, the quasi-static and dynamic compressive behaviours of a typical 304 ASS have been investigated under varying temperatures (from 20 to 600 $^{\circ}C$) and strain rates (0.001, 1000, 2000 and 3000 s^{-1}). The universal compression machine and SHPB tester equipped with an electric furnace were employed for the quasi-static and dynamic tests under elevated temperatures, respectively. The stress–strain responses,

strain rate and temperature effects and microstructural changes were obtained and analyzed. Finally, the dynamic stress–strain model considering both the temperature and strain rate is developed on the basis of the J-C model. The above results can be used for evaluation of the structural safety when subjected fire followed by an impact/explosion.

2. Experiments

2.1. Material and sample preparation

The material investigated in this work was S30408 ASS with the following chemical composition: C(0.02%), S(0.002%), P (0.033%), Si (0.46%), Mn(1.35%), Cr(18.15%), Ni(8.06%), corresponding to 304 in ASTM [28] and 1.4301 in EN 10088–1 [29]. All samples for mechanical characterization were obtained from the steel tube in the longitudinal direction using the wire-cut electrical discharge machine. In order to achieve good flatness and parallelism, the ends of SHPB samples were polished using a series of sand papers (grit dimensions: 400 to 2000 mesh). The quasi-static tensile test was conducted at room temperature with a constant 0.001 s^{-1} strain rate, according to ASTM E8/E8M-15a [30]. The engineering stress–strain relationships are depicted in Fig. 2. Due to the unobvious yield plateau, the yield stress was taken as the 0.2% proof stress in accordance with GB/T 228.1–2010 [31]. The mean Young's modulus, yield strength, ultimate tensile strength and elongation are 191.4 GPa, 261.3 MPa, 611.2 MPa and 54%, respectively. According to GB/T 34108–2017 [32], samples for quasi-static and dynamic compression tests under elevated temperatures are cylindrical in shape with dimensions of $\varnothing 5 \text{ mm} \times 5 \text{ mm}$ and $\varnothing 8 \text{ mm} \times 4 \text{ mm}$, respectively. A diameter to height ratio of 2 is designed in the dynamic compression samples to decrease the influences of friction and inertia.

2.2. Experimental setup and procedure

2.2.1. Quasi-static compression under elevated temperatures

A quasi-static compression test can serve as a basis for assessing the thermal and strain-rate effects. A total of 12 samples were tested in a

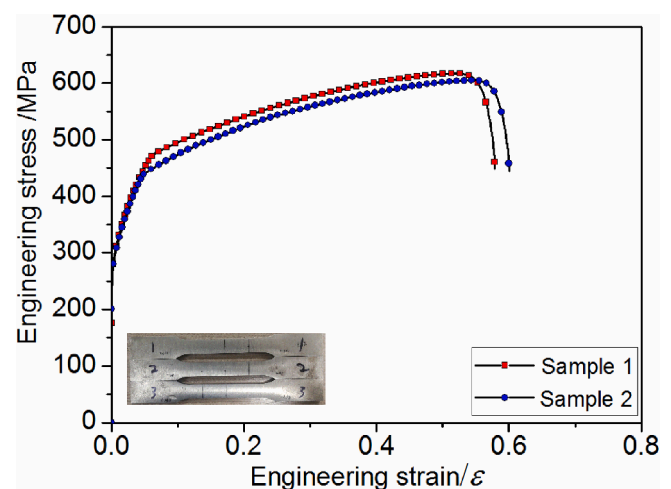


Fig. 2. Stress–strain responses of S30408 ASS under quasi-static tensile.

Table 1
Detail information in literatures [24–27].

Sources	Type	Strain rate (s^{-1})	Temperature ($^{\circ}C$)	Content
Lee et al. [24,25]	Pre-strained 304L ASS bars	2000–4000, 4000–6000	300, 500, 800	Compressive stress–strain curves, microstructure
Cadoni and Forni [26]	AISI304 ASS bars in cold forming	250, 400, 800	200, 400, 600, 800, 1000	Tensile stress–strain curves, constitutive models
Yan et al. [27]	ASTM A240/A240M 304 ASS	1000, 3000, 5000	300, 500, 700	Compressive stress–strain curves, constitutive models

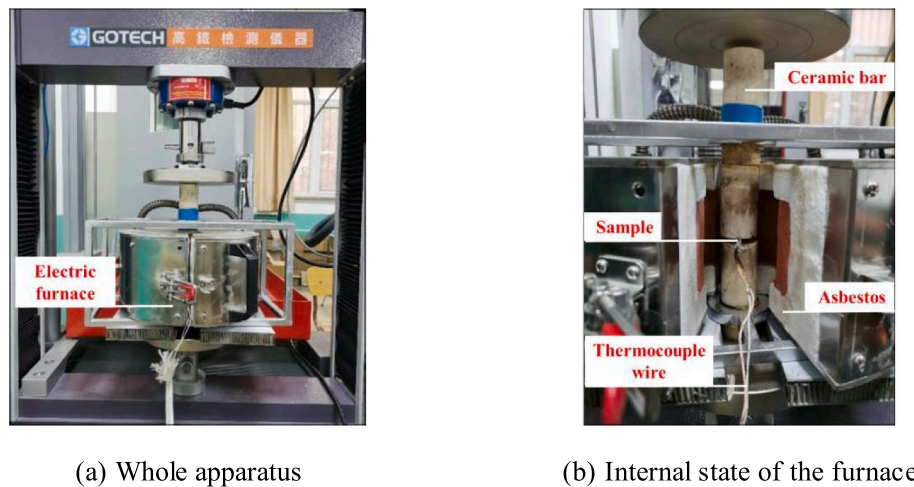


Fig. 3. Device for quasi-static compression at elevated temperatures.

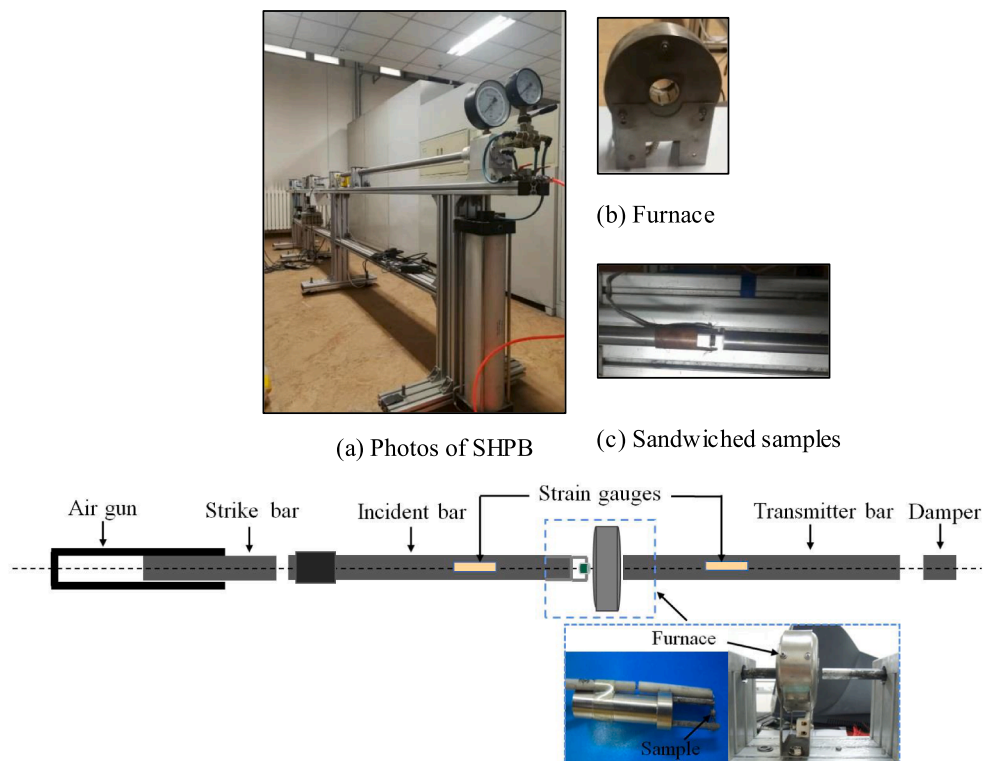


Fig. 4. Set-up for dynamic tests under elevated temperatures.

quasi-static compression regime using a 30 kN universal compression machine equipped with an electric furnace, as presented in Fig. 3. Two high-temperature resistance and high strength ceramic bars were installed to transfer the load from the testing machine to the sample. The thermocouple wire was wrapped around the sample to monitor the temperature. Samples were first heated to the target temperatures (200, 400 and 600 °C) with the speed of 2 °C/min. Then, in order to ensure a homogenous temperature within the samples, the target temperatures were held for 5 min. Finally, the samples were compressed with the rate of 0.3 mm/min to failure in a steady-state condition. The corresponding load and deformation were automatically obtained. At least three tests were performed for each strain rate and temperature, and final results were the average value of three samples.

2.2.2. Dynamic test under elevated temperatures

It is known that the SHPB device is the most widely used to measure the dynamic mechanical properties of steel material. In this work, 36 dynamic tests were performed using an SHPB tester accompanying an electric oven with a 1200 °C heating capacity. The equipment contains the air gun, strike, incident and transmitter bars, an energy-absorption apparatus and an oven. The photo and schematic view are shown in Fig. 4. The incident and transmitter bars, which are 1200 mm in length and 14 mm in diameter, are produced with 18Ni steel. The longitudinal wave speed and the Young's modulus of 18Ni steel are 5092 m/s and 210 GPa, respectively. At room temperature, the molybdenum disulfide was adopted between the contact surfaces of the sample and the bars to decrease the friction, and a copper pulse shaper was placed at the impact end of the incident bar to produce a stable wave [33]. A synchronically assembled furnace was designed to heat the sample while keeping the

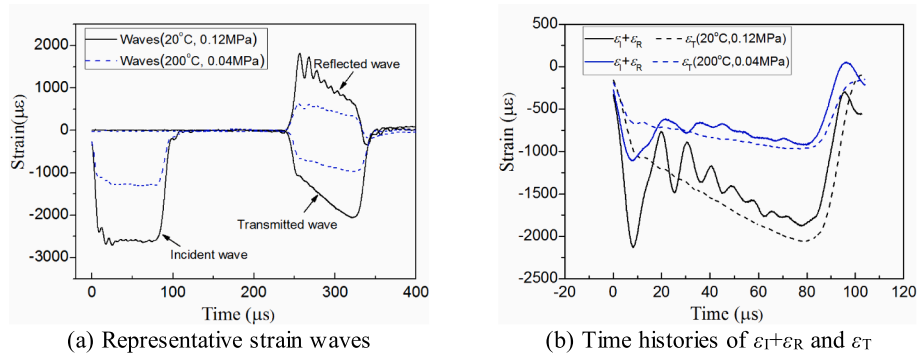


Fig. 5. Raw strain waves.

SHPB bars away from it to avoid the influence of elevated temperatures on the bars. The thermocouple was attached to the sample to measure the sample's temperature.

The experiments were performed as follows: (1) Firstly, the samples were mounted with a thermocouple sleeve and heated at a speed of 2 °C/min to the predetermined temperature followed by 5 min to achieve a uniform temperature distribution in the samples; (2) Secondly, the bars were brought into contact with the sample, and then the strike bar was fired. A similar method was also used in other high-temperature SHPB test [34]. The incident, transmitter and reflection strain waves (ϵ_I , ϵ_T and ϵ_R) were detected by the strain gauges. Based on the uniaxial elastic wave theory, the engineering strain (ϵ_{eng}), engineering stress (σ_{eng}) and strain rate ($\dot{\epsilon}$) can be calculated by Eqs. (1)–(3), respectively.

$$\epsilon_{eng} = -\frac{2C_0}{L} \int_0^t \epsilon_R dt \quad (1)$$

$$\sigma_{eng} = E_0 \frac{A_0}{A_s} \epsilon_T \quad (2)$$

$$\dot{\epsilon} = -\frac{2C_0}{L} \dot{\epsilon}_R \quad (3)$$

in which C_0 represents the velocity of the bar elastic wave, A_s and L denote the cross-sectional area and the gauge length of the sample, respectively; E_0 and A_0 represent the Young's modulus and cross-sectional area of the bars. The true strain (ϵ_{true}) and true stress (σ_{true}) are evaluated as follows:

$$\epsilon_{true} = -\ln(1 - \epsilon_{eng}) \quad (4)$$

$$\sigma_{true} = \sigma_{eng}(1 - \epsilon_{eng}) \quad (5)$$

The dynamic tests were conducted at temperatures of 20, 200, 400 and 600 °C, respectively, and averaged strain rates of 1000, 2000 and 3000 s⁻¹. Three samples were tested at each temperature and strain rate.

2.2.3. Microstructure analysis

The microstructures of the samples after both elevated temperature and impact loadings were examined using the optical microscope (Primotech, Zeiss). The samples were inlaid with a metallographic inlay machine and polished using sandpapers and polishing machine, and then etched with the aqua regia through repeated wiping. When the surface colour changes to brown, C₂H₅OH was immediately used to clean the samples for around 30 s.

3. Results and analysis

3.1. Stress–strain response

As mentioned above, the dynamic stress–strain responses were

calculated based on the strain pulses in the SHPB tests. The representative incident, reflected and transmitted strain waves (ϵ_I , ϵ_R and ϵ_T) are given in Fig. 5(a). In order to verify the stress equilibrium, the time histories of $\epsilon_I + \epsilon_R$ and ϵ_T are depicted in Fig. 5(b). As shown, the $\epsilon_I + \epsilon_R$ is approximately equal to ϵ_T under dynamic loading, which indicates that the samples are at a stress equilibrium state and the test results are reliable. It is known that keeping the strain rate constant is difficult when subjected to the quick loading. In general, the strain rate became relatively stable after experiencing the rapid-rise and obvious fluctuation stages, and similar trends were also found in other SHPB tests [35,36]. Given the unstable strain rate over the whole period, the integral averaging method suggested by Yang et al. [35] is employed to calculate the strain rate in this work.

Fig. 6 presents the averaged true stress–strain responses of 3 repeated tests deformed under varying strain rates and temperatures. The averaged curves were determined by calculating the arithmetic mean of the stress values from 3 repeated tests, as suggested by Liu et al. [37]. It is observed that the stress–strain curves significantly depend on the strain rates and temperatures. The flow stresses rise with the increasing strain rates, but an increment of temperature results in a decreasing flow stress. In addition, the stress–strain responses present a strain hardening behaviour with the increasing strains, and the strain hardening rate $d\sigma/d\epsilon$ declines with an increment of temperature. For example, at a strain rate of 2000 s⁻¹, the values of $d\sigma/d\epsilon$ are 1883, 1219, 966 and 850 MPa/unit strain under temperatures of 20, 200, 400 and 600 °C, respectively. In the subsequent analysis, the influences of temperature and strain rate on the yield stresses will be examined.

3.2. Influences of strain rate and temperature

The variations of yield stresses along with the strain rate and temperature are presented in Fig. 7(a) and (b), respectively. Since the elastic part of the stress–strain response is fluctuating, the method for extracting the dynamic yield stress is different from that adopted in the quasi-static test. Thus, the method recommended by Yang et al. [35] and Sun and Packer [38] was employed to define the dynamic yield stress, as presented in Fig. 8. It can be seen in Fig. 7 that the yield stresses are sensitive to the strain rate and temperature. For a given strain rate, the yield stress declines when the temperature increases. However, it rises with an increment of strain rate when subjected to the same temperature.

In order to quantify influences of strain rate and temperature on the dynamic compression response, the dynamic increase factor $DIF_{dy,\theta}$ and temperature reduction coefficient $k_{dy,\theta}$ of the yield stress subjected to varying strain rates and temperatures are presented in Fig. 9(a) and (b), respectively. The corresponding formulas are given as follows:

$$DIF_{dy,\theta} = f_{dy,\theta}/f_{sy,\theta} \quad (6)$$

$$k_{dy,\theta} = f_{dy,\theta}/f_{dy,20^\circ C} \quad (7)$$

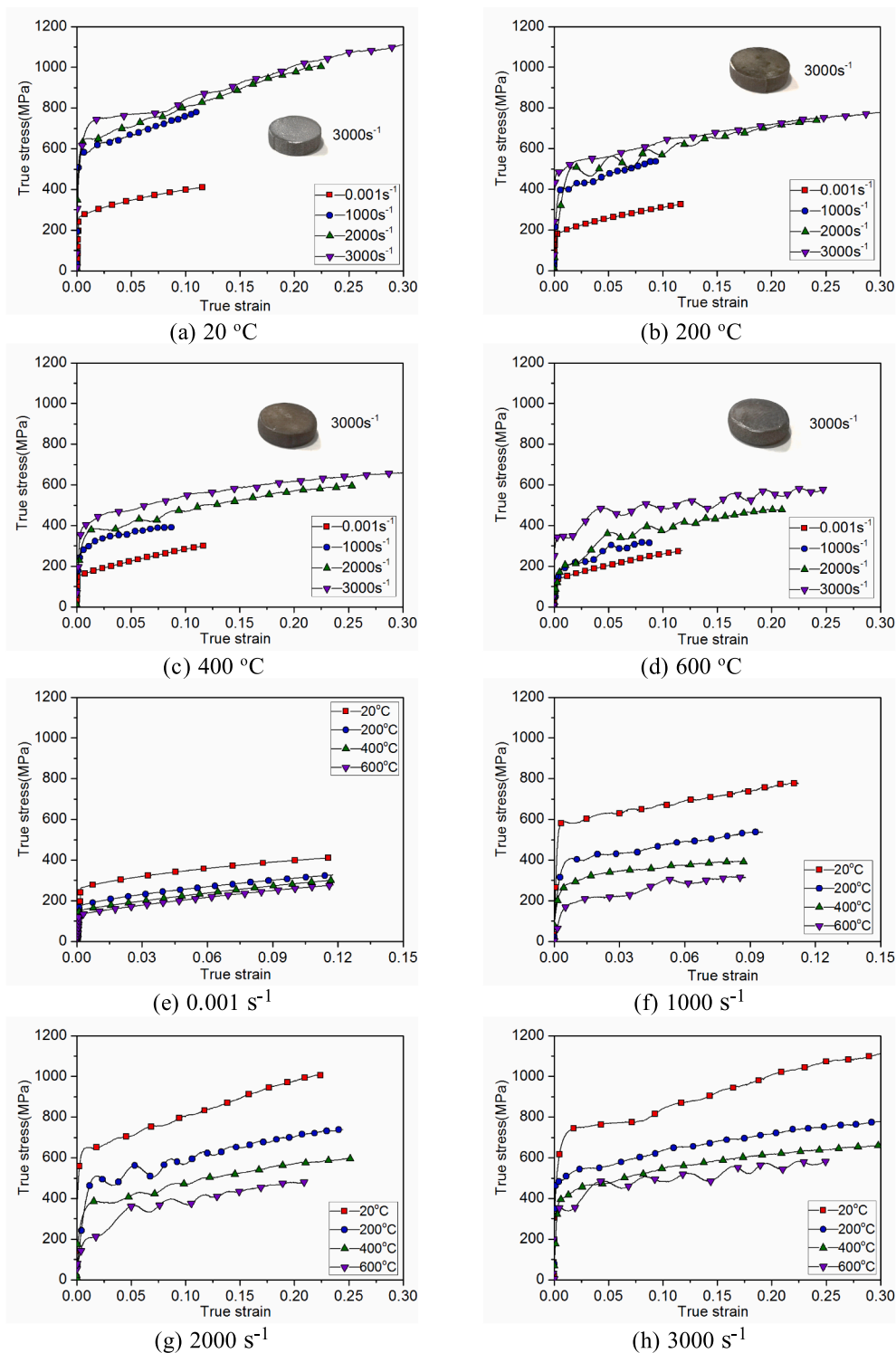


Fig. 6. True stress vs. strain responses.

in which $f_{dy,\theta}$ and $f_{dy,20^\circ C}$ are the dynamic yield stresses at elevated temperatures and ambient temperature, respectively; $f_{sy,\theta}$ represent the quasi-static yield stress under elevated temperatures.

The developments of $DIF_{dy,\theta}$ with increasing strain rates under 20, 200, 400 and 600 °C are depicted in Fig. 9(a). As presented, the $DIF_{dy,\theta}$ values under high-strain rates are greater than 1.0. In general, the highest values appear at 200 °C. The increase rate of the yield stress from 0.001 to 1000 s^{-1} is higher than that in the range of 1000–2000 s^{-1} and 2000–3000 s^{-1} . For instance, under 400 °C exposure, the yield stresses

at strain rates of 1000, 2000 and 3000 s^{-1} increased by 99%, 136% and 173%, respectively, compared to that under quasi-static strain rate. It indicates that the strengthening effect is pronounced under a high strain rate compared with the quasi-static condition. The evolution of $DIF_{dy,\theta}$ in this work is also compared with literature results, as illustrated in Fig. 9(a). The $DIF_{dy,\theta}$ values derived from the results of Lee and Lin [9] are close to those obtained in this work, while the results of Jia et al. [39] under temperatures of 172 °C are relatively low. The above results indicate that the yield stresses of S30408 ASS present an obvious strain-

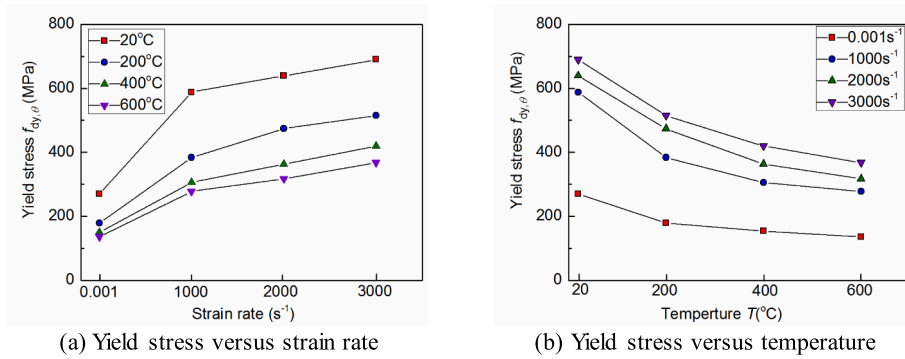


Fig. 7. Variations of yield stresses with the strain rate and temperature.

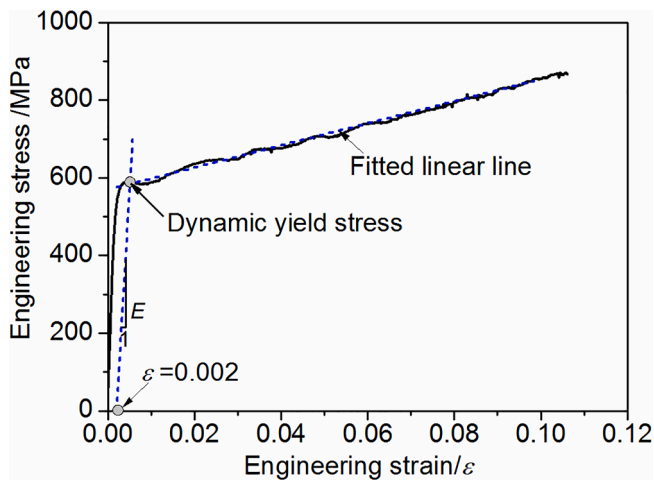


Fig. 8. Definition of dynamic yield stress.

rate effect.

The reduction factors $k_{dy,\theta}$ induced by the same temperature were higher under 2000 s^{-1} and 3000 s^{-1} than the rest, as presented in Fig. 9 (b). There are 2 phases for the yield strength degradation. The yield strength degrades fastly during 20–200 °C and gradually decline between 200 °C and 600 °C. When subjected to 200, 400 and 600 °C, the retained yield strengths under different strain rates are in the range of 65–75%, 52–61% and 47–53% of the values at ambient temperatures, respectively. Fig. 9(b) also compares the reduction factor of austenitic stainless steel suggested by Fan et al. [16] and EN 1993-1-2 [23] under the quasi-static loading. These two models are found to give reasonable predictions of the residual dynamic yield stress under varying temperatures, considering the variability in high-temperature tests.

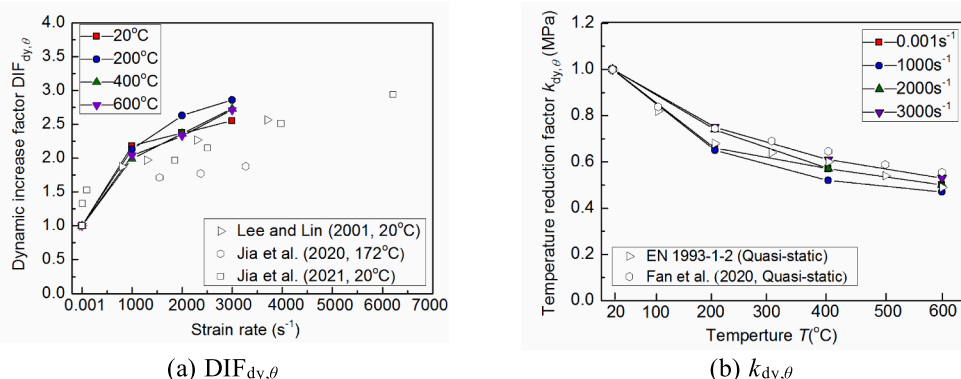


Fig. 9. Dynamic increase factors $DIF_{dy,\theta}$ and temperature reduction coefficients $k_{dy,\theta}$.

For each temperature, the influence of the strain rate on the compressive performance can be qualified via the strain-rate sensitivity coefficient β [18], defined as:

$$\beta = (\ln\sigma_2 - \ln\sigma_1) / (\ln\dot{\epsilon}_2 - \ln\dot{\epsilon}_1) \quad (8)$$

in which σ_1 and σ_2 represent the true stresses at 0.05 strain corresponding to the strain rates $\dot{\epsilon}_{\mu_1}$ and $\dot{\epsilon}_{\mu_2}$, respectively. The greater value of β indicates more sensitivity to the strain rate. Fig. 10 presents the variation of parameter β with the strain rate under different temperatures. The parameter β increases when the strain rate rises, ranging from 0.03 to 0.4. As the strain rate exceeds 1000 s^{-1} , higher temperature induces the greater value of β , especially for 400 and 600 °C.

3.3. Strain rate models

Test results have indicated that the stress–strain responses of S30408 ASS are related to the strain rate and the temperature. Therefore, a widely used temperature and rate dependence model, called the J-C model [40], is employed to predict the true stress–strain responses. This model is embedded in the finite element software by considering the influences of the strain hardening, strain rate strengthening and temperature softening, which can be written as follows:

$$\sigma = (A + B\epsilon_p^n) \left(1 + c \ln\left(\frac{\dot{\epsilon}}{\dot{\epsilon}_0}\right)\right) (1 - T^{*m}) \quad (9)$$

in which ϵ_p represents the true plastic strain; $\dot{\epsilon}_0$ and $\dot{\epsilon}_{\mu_0}$ are strain rate and quasi-static strain rate ($=0.001\text{ s}^{-1}$), respectively; T^* represents the homologous temperature ($= (T - T_R) / (T_m - T_R)$, T , T_R and T_m denote current temperature, ambient temperature and melting temperature, respectively); Parameters A , B and n denote the quasi-static stress–strain response at room temperature; Parameters c and m denote the strain-rate strengthening and thermal softening effects, respectively. Therefore, these 3 parts in each bracket are uncoupled in the model.

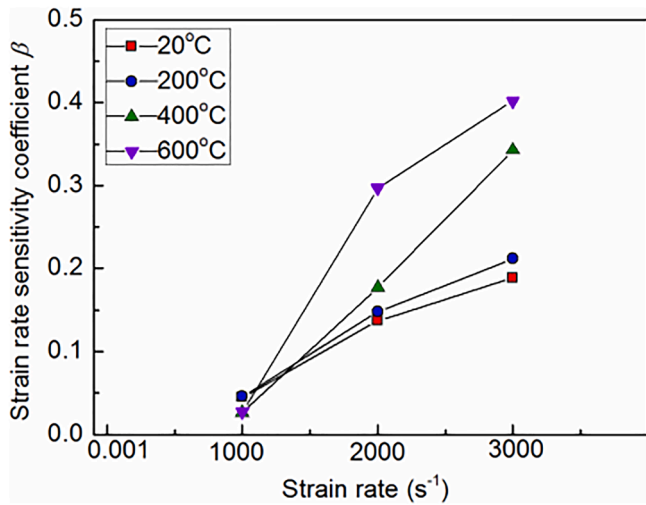


Fig. 10. Strain-rate sensitivity coefficient.

It should be noted that during SHPB tests, a temperature increment occurs due to the plastic deformation, which is recognized as the adiabatic process. The temperature rise results in the thermal softening and becomes more obvious under higher strain rate. Thus, the adiabatic temperature increment ΔT is considered in J-C model, as calculated by Eq.(10):

$$\Delta T = \frac{\beta}{\rho c_p} \int \sigma(\epsilon) d\epsilon \tag{10}$$

in which β represents the Taylor-Quineey factor taken as 0.9 in this work according to [26], ρ denotes the density (7.9 g/cm^3), c_p is the heat capacity ($500 \text{ J kg}^{-1}\text{K}^{-1}$).

By using Eq. (10), taking S30408 ASS under 3000 s^{-1} and $200 \text{ }^\circ\text{C}$ as an example, the temperature increments achieve $51.5 \text{ }^\circ\text{C}$ at strain of 0.3. Therefore, the temperature rise caused by the adiabatic process should be incorporated in the model, especially at higher strain rate.

The five parameters are determined by the test results fitting and their values are presented in Table 2, in which different values of c and m are given respectively corresponding to different strain rates and temperatures during $20\text{--}600 \text{ }^\circ\text{C}$. Fig. 11 presents the comparison between the model and test curves. In general, the model shows a reasonable agreement with the test data. Some discrepancies between test and predicted results are mainly related to some factors, such as the microstructural transformation, the adiabatic heat softening and the experimental error, etc [18,39,41].

3.4. Microstructural observation after elevated-temperature dynamic test

After compression deformation, the microstructures were examined using the optical microscopy to analyze the relationship between the elevated-temperature dynamic properties and the residual microstructure, as presented in Fig. 12. The photographs show that a higher temperature results in a pronounced increase in the grain sizes and a decline of the grain boundary area when exposed to the same strain rate.

Table 2
Fitted J-C parameters.

A(MPa)	B(MPa)	n	c	m				
				1000 s ⁻¹	2000 s ⁻¹	3000 s ⁻¹		
270	637	0.7587	0.0749	0.0921	0.1003	0.538	0.653	0.808

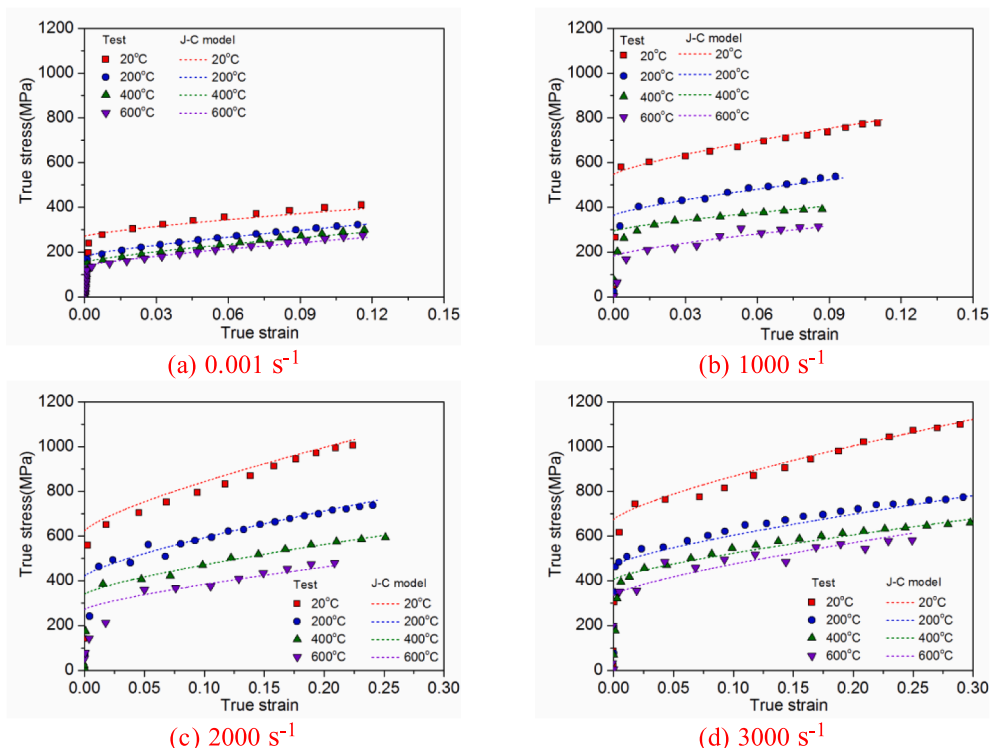


Fig. 11. Comparison between the test results and J-C model.

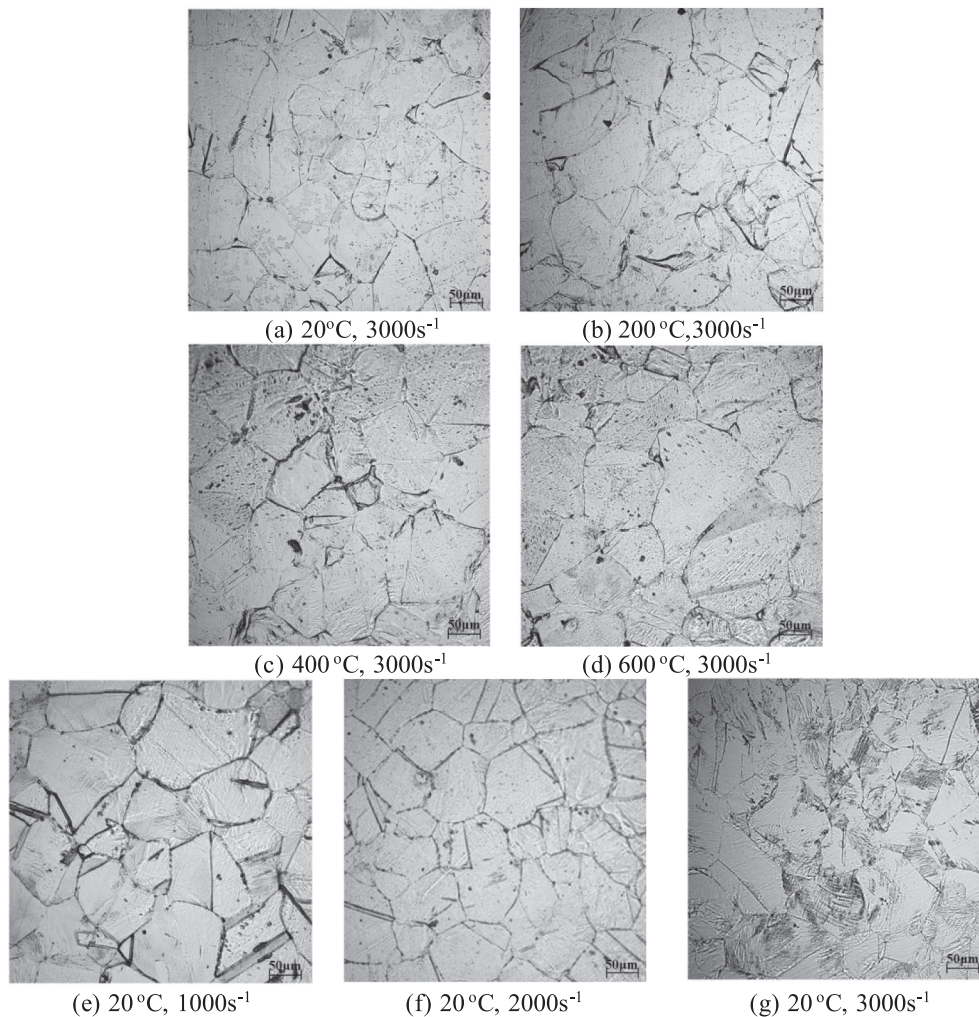


Fig. 12. Optical microstructures under different strain rates and temperatures.

Considering that the grain boundary hinders the plastic deformation and has higher strength than the inner grain, the smaller the grain boundary area is, the lower the strength and hardness are. Therefore, the inferior mechanical responses of S30408 ASS were obtained at higher temperatures. In addition, as the strain rate increases, the average grain dimension decreases while the grain boundary gradually diffuses and become irregular. Therefore, the rise in the grain boundary area under a higher strain rate benefits the mechanical performance. In general, the grains maintain a well integrity structure, and the changes in the grain shape are unobvious under varying temperatures and strain rates, indicating a good performance of S30408 ASS under coupled fire and impact loadings.

4. Conclusions

This study investigated the quasi-static and dynamic compressive behaviours of S30408 austenitic stainless steel (ASS) under temperatures of 20, 200, 400 and 600 °C and strain rates ranged from 0.001 s⁻¹ to 3000 s⁻¹. According to the test and analyses, the main conclusions are obtained:

- (1) The compressive responses of S30408 ASS are sensitive to the strain rate and temperature. The yield stress increases with an increment of the strain rate, but declines with increased temperatures. In addition, the rate of the strain hardening becomes weaker at higher temperatures.

- (2) As the strain rate rises from 0.001 s⁻¹ to 3000 s⁻¹, the elevated-temperature dynamic increase factors $DIF_{dy,\theta}$ rises, with the maximum value of 2.86 under 200 °C and 3000 s⁻¹. The temperature reduction coefficients $k_{dy,\theta}$ decreases significantly during 20–200 °C and the reduction slows down from 200 to 600 °C. S30408 ASS maintains 47–53% of its normal-temperature yield strengths under 600 °C. The strain-rate sensitivity coefficient is more pronounced under a higher strain rate and a higher temperature.
- (3) Based on the experimental results, the parameters for J-C constitutive model considering the adiabatic temperature increment were determined under 20–600 °C. This model could be used to predict the residual performance of structures made with this type of steel under the coupled action of fire and impact/blast loadings.
- (4) Residual microstructure indicates that higher temperatures result in an obvious rise of the grain size, while the increase in the strain rate decreases the grain size. In general, the moderate grain deformation occurs under coupled high temperatures and strain rates within the parameter range in this work.

Declaration of Competing Interest

The authors declare that they have no known competing financial interests or personal relationships that could have appeared to influence the work reported in this paper.

Acknowledgements

The study was supported by the China Postdoctoral Science Foundation (2020M670656) and Fund Program for the Scientific Activities of Selected Returned Overseas Professionals in Shanxi Province (20210010).

References

- [1] Han LH, Xu CY, Tao Z. Performance of concrete filled stainless steel tubular (CFSSST) columns and joints: Summary of recent research. *J Constr Steel Res* 2019; 152:117–31.
- [2] Zhao H, Wang R, Hou CC, Lam D. Performance of circular CFDST members with external stainless steel tube under transverse impact loading. *Thin-Walled Struct* 2019;145:106380.
- [3] Azad SK, Li DX, Uy B. Axial slenderness limits for austenitic stainless steel-concrete composite columns. *J Constr Steel Res* 2020;166:105856.
- [4] Kucukler M, Xing Z, Gardner L. Behaviour and design of stainless steel I-section columns in fire. *J Constr Steel Res* 2020;165:105890.
- [5] Arrayago I, Rasmussen KJR, Real E. Statistical analysis of the material, geometrical and imperfection characteristics of structural stainless steels and members. *J Constr Steel Res* 2020;175:106378.
- [6] Zhao H, Wang R, Lam D, Hou C-C, Zhang R. Behaviours of circular CFDST with stainless steel external tube: Slender columns and beams. *Thin-Walled Struct* 2021; 158:107172. <https://doi.org/10.1016/j.tws.2020.107172>.
- [7] CECS 410: 2015, Technical Specification for Stainless Steel Structure, Planning Press of China, Beijing, 2015 (In Chinese).
- [8] EN 1993-1-4:2006+A1: 2015. Eurocode 3—Design of Steel Structures Part1–4: General Rules-Supplementary Rules for Stainless Steel. British Standards Institution. London, UK, 2015.
- [9] Lee WS, Lin CF. Impact properties and microstructure evolution of 304L stainless steel. *Mater Sci Eng A* 2001;308:124–35.
- [10] Lichtenfeld JA, Van Tyne CJ, Mataya MC. Effect of strain rate on stress-strain behavior of alloy 309 and 304L austenitic stainless steel. *Metall Mater Trans A* 2006;37(1):147–61.
- [11] Zhou F, Young B. Experimental and numerical investigations of cold-formed stainless steel tubular sections subjected to concentrated bearing load. *J Constr Steel Res* 2007;63(11):1452–66.
- [12] Abdella K. Explicit full-range stress-strain relations for stainless steel at high temperatures. *J Constr Steel Res* 2009;65(4):794–800.
- [13] Cadoni E, Fenu L, Forni D. Strain rate behaviour in tension of austenitic stainless steel used for reinforcing bars. *Constr Build Mater* 2012;35:399–407.
- [14] Zhou F, Li L. Experimental study on hysteretic behavior of structural stainless steels under cyclic loading. *J Constr Steel Res* 2016;122:94–109.
- [15] Liu M, Fan S, Ding R, Chen G, Du E, Wang K. Experimental investigation on the fire resistance of restrained stainless steel H-section columns. *J Constr Steel Res* 2019; 163:105770. <https://doi.org/10.1016/j.jcsr.2019.105770>.
- [16] Fan S, Ding R, Zheng J, Xie F, Wu Q. Refined model for the stress-strain curve of austenitic stainless-steel materials at elevated temperatures. *J Mater Civ Eng* 2020; 32(4):04020032. [https://doi.org/10.1061/\(ASCE\)MT.1943-5533.0003091](https://doi.org/10.1061/(ASCE)MT.1943-5533.0003091).
- [17] Fernando D, Teng JG, Quach WM, De Waal L. Full-range stress-strain model for stainless steel alloys. *J Constr Steel Res* 2020;173:106266. <https://doi.org/10.1016/j.jcsr.2020.106266>.
- [18] Jia S, Tan Q, Ye J, Zhu Z, Jiang Z. Experiments on dynamic mechanical properties of austenitic stainless steel S30408 and S31608. *J Constr Steel Res* 2021;179: 106556. <https://doi.org/10.1016/j.jcsr.2021.106556>.
- [19] Martins AD, Gonçalves R, Camotim D. Numerical simulation and design of stainless steel columns under fire conditions. *Eng Struct* 2021;229:111628. <https://doi.org/10.1016/j.engstruct.2020.111628>.
- [20] Yuan HX, Liu XH, Liu JL, Theofanous M. Cyclic behaviour and hysteretic model of austenitic stainless steel bolted T-stubs. *J Constr Steel Res* 2021;182:106659.
- [21] Forni D, Chiaia B, Cadoni E. High strain rate response of S355 at high temperatures. *Mater Des* 2016;94:467–78.
- [22] Cadoni E, Forni D. Mechanical behaviour of a very-high strength steel (S960QL) under extreme conditions of high strain rates and elevated temperatures. *Fire Saf J* 2019;109:102869. <https://doi.org/10.1016/j.firesaf.2019.102869>.
- [23] BS EN 1993-1-2, Eurocode 3: Design of steel structures: Part 1-2: General rules-Structural fire design, BSI, London, 2005.
- [24] Lee WS, Lin CF, Chen TH, Yang MC. High temperature microstructural evolution of 304L stainless steel as function of pre-strain and strain rate. *Mater Sci Eng A* 2010; 527:3127–37.
- [25] Lee W-S, Lin C-F, Chen T-H, Yang M-C. Effects of prestrain on high temperature impact properties of 304L stainless steel. *J Mater Res* 2010;25(4):754–63.
- [26] Cadoni E, Forni D. Austenitic stainless steel under extreme combined conditions of loading and temperature. *J Dynamic Behav Mater* 2019;5(3):230–40.
- [27] Yan QS, Lv CX, Sun BW, Yang L. Dynamic mechanical behavior at elevated temperatures and high strain rate of structural stainless steel used in civil engineering. *J Mater Civ Eng* 2020;32(5):04020094.
- [28] A1022/A1022M-16b, Standard specification for deformed and plain stainless steel wire and welded wire for concrete reinforcement. ASTM International, United States, 2016.
- [29] EN 10088-1: 2014, Stainless steels-Part 1: List of stainless steels, European committee for standardization, Brussels, 2014.
- [30] American Society for Testing and Materials (ASTM), Standard test methods for tension testing of metallic materials, E8/E8M-15a. West Conshohocken, USA, 2015.
- [31] GB/T 228.1-2010, Metallic materials-Tensile testing-Part 1 Method of test at room temperature. China Architecture & Building Press, Beijing, China, 2010.
- [32] GB/T 34108-2017, Code for metallic materials-high strain rate compression method at ambient temperature, Standards Press of China, Beijing, China, 2017.
- [33] Mei Y, Ban H. High strain rate behaviour of stainless-clad bimetallic steel. *Eng Struct* 2020;207:110219. <https://doi.org/10.1016/j.engstruct.2020.110219>.
- [34] Ponnusamy P, Masooda SH, Ruan D, Palanisamy S, Rashid RAR, Mukhlis R, et al. Dynamic compressive behaviour of selective laser melted AlSi12 alloy: Effect of elevated temperature and heat treatment. *Addit Manuf* 2020;36:101614.
- [35] Yang XQ, Yang H, Zhang SM. Rate-dependent constitutive model of S690 high-strength structural steel. *Constr Build Mater* 2019;198:597–607.
- [36] Zhu Y, Yang H, Zhang SM. Dynamic mechanical behavior and constitutive models of S890 high-strength steel at intermediate and high strain rates. *J Mater Eng Perform* 2020;29:6727–39.
- [37] Liu XY, He ZY, Ye JY, Yan LH, Li S, Tang Y. Study on dynamic mechanical behaviour of Q460JSC and HQ600 high strength steel. *J Constr Steel Res* 2020;173: 106232.
- [38] Sun M, Packer JA. High strain rate behavior of cold-formed rectangular hollow sections. *Eng Struct* 2014;62:181–92.
- [39] Jia B, Rusinek A, Pesci R, Bahi S, Bernier R. Thermo-viscoplastic behavior of 304 austenitic stainless steel at various strain rates and temperatures: Testing, modeling and validation. *Int J Mech Sci* 2020;170:105356.
- [40] Johnson GR, Cook WH. A constitutive model and data for metals subjected to large strains, high strain rates and high temperatures, Den Haag. In: The Netherlands Proceedings of the 7th International Symposium on Ballistics; 1983. p. 541–7.
- [41] Fan XL, Suo T, Sun Q, Wang TJ. Dynamic mechanical behavior of 6061 AL alloy at elevated temperatures and different strain rates. *Acta Mech Solida Sin* 2013;26: 111–20.